Secondary Organic Aerosols from OH Oxidation of Cyclic Volatile Methyl Siloxanes as an Important Si Source in the Atmosphere

Chong Han[1,2], Hongxing Yang[1], Kun Li[2,3], Patrick Lee[2], John Liggio[2], Amy Leithead[2], Shao-Meng Li[4]*

[1]School of Metallurgy, Northeastern University, Shenyang, 110819, China

[2]Air Quality Research Division, Environment and Climate Change Canada, Toronto, Ontario M3H 5T4, Canada

[3]Laboratory of Atmospheric Chemistry, Paul Scherrer Institute, Villigen 5232, Switzerland

[4]State Key Joint Laboratory of Environmental Simulation and Pollution Control, College of Environmental Sciences and Engineering, Peking University, Beijing, China 100871

Correspondence: Shao-Meng Li (shaomeng.li@pku.edu.cn)

Short summary: We presented yields and compositions of Si-containing SOA generated from the reaction of cVMS (D3-D6) with OH radicals. NO_x played negative roles on cVMS SOA formation, while ammonium sulfate seeds enhanced D3-D5 SOA yields at short photochemical ages under high-NO_x conditions. The aerosol mass spectra confirmed that the components of cVMS SOA significantly relied on OH exposure. A global cVMS-derived SOA source strength was estimated to understand SOA formation potentials of cVMS.

Abstract

Cyclic volatile methyl siloxanes (cVMS) are active ingredients in widely used consumer products, which can volatilize into the atmosphere, thus attracting much attention due to their potential environmental risks. While in the atmosphere the cVMS undergo oxidation yielding both gaseous and particulate products. The aerosol yields and compositions from the OH oxidation of four cVMS (D3-D6) were determined under low

and high-NO_x conditions in an oxidation flow reactor. The aerosol yields progressively increased from D3 to D6, consistent with the volatilities and molecule weights of these cVMS. NO_x can restrict the formation of SOA, leading to lower SOA yields under high-NO_x conditions than under low-NO_x conditions, with a yield decrease between 0.05-0.30 depending on the cVMS. Ammonium sulfate seeds exhibited minor impacts on SOA yields under low-NO_x conditions, but significantly increased the SOA yields in the oxidation of D3-D5 at short photochemical ages under high-NO_x conditions. The mass spectra of the SOA showed a dependence of its chemical compositions on OH exposure. At high exposures, equivalent to photochemical ages of >6 days in the atmosphere, D4-D6 SOA mainly consisted of C_xH_y and $C_xH_yO_zSi_n$ under low-NO_x conditions, whereas they primarily contained N_mO_z, C_xH_y, $C_xH_yO_1$, $C_xH_yO_{>1}$ and $C_xH_yO_zSi_n$ under high-NO_x conditions. The potential contributions of cVMS to SOA formation in the atmosphere were evaluated using the reported cVMS annual production and the yield data obtained at the longest equivalent days in the present study. A global cVMS-derived SOA source strength is estimated to be 0.16 Tg yr^{-1}, distributed over major urban centers.

1 Introduction

Secondary organic aerosols (SOA), which contribute 50-85% to the mass of atmospheric organic aerosols (OA) (Glasius and Goldstein, 2016), are mainly formed via the partitioning of low volatility products from oxidation of volatile organic compounds (VOCs), semi- and intermediate volatile organic compounds(S/IVOCs) (Riipinen et al., 2012). SOA has attracted significant attention due to their important impacts on climate, ecosystems and human health (Berndt et al., 2016). Global budgets of SOA remain an unresolved issue despite extensive research, largely due to uncertainties associated with aerosol yields and the presence of unconsidered SOA precursors.

As one type of anthropogenic VOC and potential SOA precursors, cyclic volatile methyl siloxanes (cVMS) are widely used in industrial applications and personal care products (Genualdi et al., 2011; Krogseth et al., 2013a). cVMS have been classified as high-volume chemicals with an annual production of millions of tons globally (Rücker and Kümmerer, 2015; Ahrens et al., 2014). Studies of cVMS in the environment have focused on investigating health and environmental impacts particularly due to their potential persistence, bioaccumulation and toxicity (Guo et al., 2019; Liu et al., 2018; Farasani and Darbre, 2017; Xu et al., 2019; Kim et al., 2018; Coggon et al., 2018). As a result, the European Council has proposed a restriction on the octamethylcyclotetrasiloxane (D4) and decamethylcyclopentasiloxane (D5) content in wash-off personal care products to a limit of 0.1 mass% by 2020 (Eur-Lex, 2018). The legislative actions notwithstanding, knowledge of environmental behavior of cVMS still needs to be further deepened as compared to their applications and economic significance (Rücker and Kümmerer, 2015).

It has been estimated that approximately 90% of cVMS are emitted into the atmosphere due to their high saturation vapor pressures (Allen et al., 1997). Gas-phase cVMS have been observed in both indoor and outdoor air. Tang et al. (2015) reported that cVMS accounted for about one third of total VOC mass concentration in a classroom. Outdoor air concentrations of cVMS have also been measured at different sites worldwide (Li et al., 2020; Wang et al., 2018; Rauert et al., 2018), increasing from rural to urban sites and consistent with increasing population density (Rücker and Kümmerer, 2015). For example, at a rural site in Sweden, the concentration of hexamethylcyclotrisiloxane (D3), D4, D5 and dodecamethylcyclohexasiloxane (D6) were 0.94, 3.5, 13 and 1 ng/m^3, respectively (Kierkegaard and Mclachlan, 2013), while they were 18, 55, 172 and 14 ng/m^3 in urban areas of Toronto in Canada, respectively (Genualdi et al., 2011; Rauert et al., 2018). cVMS have also been detected in the remote Arctic atmosphere, confirming their long-range transport (Genualdi et al., 2011; Krogseth et al., 2013b). Atmospheric half-lives of cVMS are on the order of 30, 15,

10 and 6 days for D3-D6, respectively, which allow cVMS to exhibit a hemispherical distribution in the atmosphere (Canada, 2008; Xiao et al., 2015). These lifetimes are driven mostly by reactions with the OH radicals (Xiao et al., 2015; Wang et al., 2013), which generate silanols and dimeric products that can be partitioned to condensed phases (Coggon et al., 2018; Sommerlade, 1993; Wu and Johnston, 2016). Different OH concentrations can partly explain the seasonal variation of cVMS lifetimes that was characterized by longer during winter than in summer (Rücker and Kümmerer, 2015). The loss of cVMS in the atmosphere is negligible through O_3 and NO_3 due to their small reaction rates (Atkinson, 1991). The global loss by the reaction with Cl atoms is less than 5 % on account of low Cl concentrations, although it may be higher in some regions where cVMS emissions and Cl sources overlap in both space and time (Alton and Browne, 2020). It has been demonstrated that elemental Si is a frequent constituent of nanoparticles in rural and urban areas (Phares et al., 2003; Rhoads, 2003; Bein, 2005; Bzdek et al., 2014) and in remote regions (Li and Winchester, 1990; Li and Winchester, 1993). These Si-containing nanoparticles have previously been attributed to ore smelting processes, but recent studies have shown that Si-containing species are one of the main components in cVMS SOA, suggesting that the oxidation of cVMS may be an important source of Si in atmospheric aerosols (Wu and Johnston, 2016, 2017). In a modeling study, the oxidation products of cVMS (D4, D5 and D6) were considered to quantify the maximum potential for aerosol formation through reactions with the OH radicals (Janechek et al., 2017). Chandramouli and Kamens (2001) demonstrated the gas-particle partitioning of silanols from D5 oxidation by the OH radicals. Wu and Johnston (2016, 2017) analyzed the chemical composition of secondary aerosols from OH oxidation of D4 and D5, showing a large number of monomeric and dimeric products. Janechek et al. (2017, 2019) reported physical properties of SOA generated by OH oxidation of D5, including hygroscopicity, cloud seeding potential and volatility. Charan et al. (2022) measured SOA yields of D5 using chambers and flow tube reactors, emphasizing the

89 importance of the relevant OH concentrations and exposures when extrapolating these laboratory results or
90 comparing with other studies. These studies mainly focused on D5 and occasionally D4 but rarely others. To
91 better understand the SOA-forming potentials of typical cVMS in the atmosphere, accurate yields and
92 molecular compositions of SOA from the oxidation of cVMS under various atmospheric conditions are
93 needed.

94 In this work, the formation of SOA from the oxidation of four cVMS (D3-D6) by OH radical was
95 investigated in an oxidation flow reactor (OFR). Under various combinations of NO_x and ammonium sulfate
96 seed concentrations, the yields and compositions of SOA formed from the oxidation were measured using a
97 suite of instruments including a scanning mobility particle sizer (SMPS), a proton transfer reaction time of
98 flight mass spectrometer (PTR-ToF-MS) and an aerosol mass spectrometer (AMS). Based on these SOA
99 yields, the contribution of cVMS to SOA in the global atmosphere was estimated using reported cVMS
100 concentrations. The results obtained here can largely improve our understanding of the contribution and
101 composition of SOA from cVMS.

102 **2 Experiments and methods**

103 **2.1 Photo-oxidation experiments**

104 The reactions of cVMS with OH radicals were controlled at a constant temperature (21±1˚C) and relative
105 humidity (35%±2%) in a custom-made oxidation flow reactor (the Environment and Climate Change Canada
106 oxidation flow reactor, ECCC-OFR), which is shown in Fig. S1 of the Supplement and has been described
107 in detail previously (Li et al., 2019a). Briefly, the ECCC-OFR is a fused quartz cylinder (length: 50.8 cm,
108 inner diameter: 20.3 cm) equipped with a conical inlet and 7 outlets. Wall losses of particles and gases in the
109 ECCC-OFR have been shown to be lower than in other OFRs (Huang et al., 2017; Lambe et al., 2011;
110 Simonen et al., 2017; Li et al., 2019a). The length and full angle of cone inlet are 35.6 cm and 30°,

111 respectively, designed to minimize the formation of jetting and recirculation in the OFR. The outlet at the
112 reactor center is a stainless-steel sampling port (inner diameter: 0.18 in) extending 12.7 cm long into the
113 ECCC-OFR. This sampling inlet reduces the impact of potential turbulent eddies caused by the back end of
114 the reactor. The remaining 6 outlets around the perimeter are designed to allow side flows to pass through
115 the OFR as a sheath flow, indirectly reducing wall losses of gases and particles inside the OFR upon sampling.
116 Ozone-free mercury UV lamps for generating OH radicals are housed in small quartz tubes around and in
117 parallel to the quartz reaction cylinder, and a large flow of air through each of these smaller quartz tubes is
118 used to remove the heat produced by the lamps. The relative humidity was adjusted by controlling the ratio
119 of dry air to wet air into the reactor, and was measured using a humidity sensor (Vaisala) at one of the sheath
120 flow outlets (side flows) of the reactor. The volume of the entire ECCC-OFR is about 16 L and the total flow
121 rate is 8 L min^{-1}, leading to a residence time of 2 min in the OFR.

122 OH radicals were produced through the reaction of water vapor with $O(^1D)$ formed from O_3 photolysis at
123 254 nm. The OH concentration in the ECCC-OFR was regulated by controlling the input voltage and the
124 number of UV lamps. Methanol vapor, introduced into the ECCC-OFR through a bubbler containing
125 methanol solution, was used to determine the OH exposure (i.e., photochemical age, from the multiplication
126 of OH concentration and reaction time) by tracking its decay in the reactor from the reaction with the OH.
127 The decay, or fractional loss, of gas-phase methanol, $[MeOH]/[MeOH]_0$ was measured with the PTR-ToF-
128 MS, and was used to calculate the OH concentration via Equation 1,

129 $$[OH]=-\frac{1}{k_{MeOH}}\ln\frac{[MeOH]}{[MeOH]_0} \quad (1)$$

130 where k_{MeOH} is the second-order rate constant of methanol reaction with OH at 298 K (9.4×10^{-13} cm^3
131 $molecule^{-1}$ s^{-1}). It was noted that the OH exposure measurement was offline, because methanol can affect the
132 OH reactivity with cVMS. Under low and high-NO_x conditions described below, the OH exposure varied in

the range of 5.5×10^{10}-1.8×10^{12} and 8.2×10^{10}-1.1×10^{12} molecules cm^{-3} s, respectively. They correspond to 0.4-14.2 and 0.6-8.5 equivalent days (photochemical age), respectively, assuming that an average OH concentration in air is 1.5×10^{6} molecules cm^{-3} (Mao et al., 2009).

Pure D3-D6 cVMS compounds (solid D3 and liquid D4, D5 and D6) were placed in a glass U-type tube and maintained at the room temperature. Vapors from these compounds (Table S1 of the Supplement) were separately introduced into the ECCC-OFR by a small flow of zero air (1-18 mL min^{-1}) passing over the headspace of the U-tube containing the pure compounds. The concentrations of D3-D6 in the ECCC-OFR ranged from 20 to 43 ppb (Table S2), depending on their volatilities. Table S2 summarizes the concentrations of cVMS at the reactor inlet and outlet, when the OH exposure was 1.85×10^{12} and 1.10×10^{12} molecules cm^{-3} s in low and high-NO_x experiments, respectively, indicating the reaction depth of cVMS. To study the influence of existing particles on the SOA formation, ammonium sulfate (AS) seed particles were produced using an atomizer, dried by a diffusion dryer and neutralized by a neutralizer and injected into the reactor without size selection. The mass concentration of AS seed particles was approximately 30 μg m^{-3} for all experiments.

N_2O was used as a source of NO to achieve high-NO_x conditions (Lambe et al., 2017). NO_x conditions were defined by the fate of peroxy radicals (RO_2), which was described by the reaction rate ratio (R_{NO}) of RO_2 + NO and RO_2 + HO_2 (Peng et al., 2018). The R_{NO} ratio increases with increasing OH exposures at a constant concentration of N_2O (Li et al., 2019b). To achieve a constant branching ratio during the high-NO_x experiments, the initial N_2O concentration in the OFR was varied (1.6%-8.0%) to maintain an R_{NO} value of 20 (Li et al., 2019b), as calculated using a model (OFR Exposures Estimator v3.1) (Peng et al., 2018). A ratio of R_{NO}=20 indicates that 95% of RO_2 reacts with NO, ensuring the dominance of RO_2 + NO, which represents conditions that are relevant for urban atmosphere (Peng et al., 2019). The role of RO_2 + RO_2 here

should be minor or negligible due to the low concentration of SOA precursors (cVMS, 18-46 ppb) (Lambe et al., 2017; Peng et al., 2019; Li et al., 2019b). Peng et al. (2019) have reported that in the experiments utilizing the injection of N_2O to achieve high-NO_x conditions, the relative importance of RO_2 + OH was generally negatively correlated with N_2O due to the suppressing effect of NO_x on OH radicals and the increasing role of RO_2 + NO. Under low-NO_x conditions, N_2O was not introduced into the OFR, where the reaction ratio of RO_2 with HO_2 was estimated to be larger than 99% according to the model mentioned above (Peng et al., 2018), representing atmospheric scenarios with few NO_x sources.

2.2 Characterization and analysis

The concentrations of cVMS in the OFR were measured online with PTR-ToF-MS (Ionicon Analytik GmbH) (Liggio et al., 2016). The number and mass size distribution of aerosols was monitored using a scanning mobility particle sizer (SMPS, TSI). The mass spectra and elemental composition of aerosols was determined with a high-resolution time-of-flight aerosol mass spectrometer (HR-ToF-AMS, Aerodyne) and analyzed with the AMS analysis software Squirrel (version 1.62G) and Pika (version 1.22G).

SOA mass yields (Y) were calculated via Equation 2,

$$Y = \frac{\Delta C_{SOA}}{\Delta C_{cVMS}} \quad (2)$$

where ΔC_{SOA} and ΔC_{cVMS} are the mass concentrations of SOA formed and cVMS lost, respectively. The mass concentration of SOA was determined by multiplying the effective aerosol density by the integrated SOA volume concentration from the SMPS, subtracting the AS seed volume for experiments with AS seeds. The effective aerosol density (ρ) was calculated for unseeded experiments through the following Equation 3 (Lambe et al., 2015),

$$\rho = \frac{D_{va}}{D_m} \quad (3)$$

where D_{va} is the vacuum aerodynamic diameter obtained from the HR-ToF-AMS, and D_m is the electric

mobility diameter measured by the SMPS. The ρ varied in the range of 1.6-1.8 depending on the cVMS. The same ρ value was also used in the seeded experiments. It should be pointed out that the background values in Table S3 have been subtracted when calculating the cVMS SOA yields. The average data of SMPS and AMS in the last ~10 minutes for each OH exposure was used to calculate the SOA yields (inset of Fig S2), which can reduce the deviation caused by unstable SOA loadings at high OH exposures.

3 Results and discussion

3.1 SOA yields

Taking the D5 SOA under unseeded conditions as an example, the number and mass size distributions of aerosols were shown in Fig. S3 at three photochemical ages (PA), i.e., time-integrated OH exposure. It can be seen that small particles dominated the total particle number counts, while large ones dominated the mass. The mass mode diameter of SOA for mass size distributions increased with PA under low and high-NO_x conditions. The mass concentrations and time series of SOA obtained from SMPS and AMS were shown in Table S4 and Fig. S2, respectively, which reflected a step-by-step pattern with increasing OH exposures. Unstable SOA loadings at high OH exposures may be attributed to the fragmentation reactions, leading to the difficulty in the deposition of products on SOA.

Figure 1 shows the SOA yields from the photooxidation of the D3-D6 cVMS under low and high-NO_x conditions as a function of PA, with and without AS seed particles. SOA yields have been widely used to estimate the potential of precursors to produce aerosol mass (Mcfiggans et al., 2019; Li et al., 2019a; Bruns et al., 2015; Lambe et al., 2015). As shown in Fig. 1, the cVMS SOA yields exhibited an overall increasing trend with PA, expressed in equivalent photochemical days, which agreed with the trend of D5 SOA yields reported by Janechek et al. (2019). Under low-NO_x conditions (Fig. 1a), SOA yields exhibited a slow growth, reaching a plateau after 10 equivalent days. This may be due to increased gas-phase fragmentation of cVMS

to generate some higher volatility products, leading to a small increasing amplitude of partition ratio of species into SOA at longer photochemical ages.

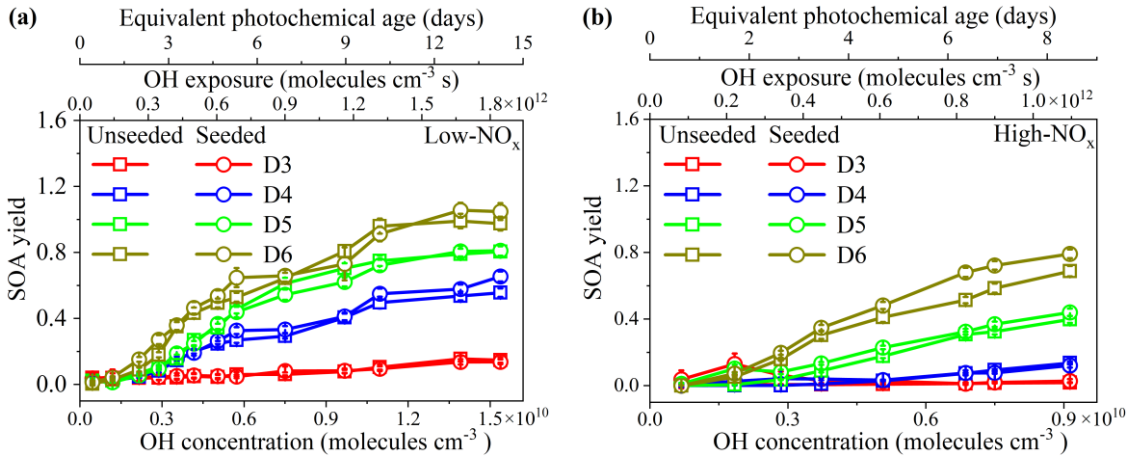

Figure 1. SOA yields from unseeded and seeded (30 μg m^{-3}) photooxidation of cVMS by OH radicals. **(a)** low-NO_x experiments; **(b)** high-NO_x experiments.

For the unseeded and low-NO_x experiments in Fig. 1a, SOA yields of four cVMS exhibited significant differences in values over the same number of equivalent days. The SOA yields successively increased from D3 to D6, consistent with the volatilities and molecular masses of the cVMS as well as their reaction rate constants with the OH radical (Alton and Browne, 2020; Kim and Xu, 2017; Safron et al., 2015). The maximum SOA yields of D3-D6 were (0.16±0.02), (0.56±0.03), (0.80±0.03) and (0.99±0.04), respectively, occurring after a PA of 12 equivalent days. It has been reported that D5 SOA yields varied in the range of 0-1.1 (Janechek et al., 2019; Wu and Johnston, 2017; Charan et al., 2022). Under a low OH exposure (~10^{10}-10^{11} molecules cm^{-3} s), the D5 SOA yield (0.01-0.11) obtained here was similar to that (chamber, 0-0.057; flow tube, 0.018-0.06) measured by Charan et al. (2022). However, under a high OH exposure of ~10^{11}-10^{12} molecules cm^{-3} s, the D5 SOA yield of 0.46-0.70 was higher than 0.22 and 0.14-0.35 (flow tube) reported by Janechek et al. (2019) and Charan et al. (2022), respectively, which may be attributed to differences in experimental conditions, such as differences in reactors, wall losses, SOA measurement methods,

determination of OH concentrations, and initial D5 concentrations (Table S5) (Janechek et al., 2019; Charan et al., 2022). Although the amount of cVMS lost was variable, cVMS SOA yields positively depended on SOA mass concentrations (Fig. S4), and this trend was observed in previous D5 SOA experiments with OH oxidation (Wu and Johnston, 2017).

As shown in Fig. 1b, the order of SOA yields from the four cVMS under high-NO_x conditions was the same as that under low-NO_x conditions. However, the SOA yields under high-NO_x conditions were generally smaller than the corresponding yields at similar OH exposures under low-NO_x conditions, with a decrease of 0.05-0.30 depending on the cVMS. Such a reduction suggests that NO_x can restrict the formation of cVMS SOA. NO_x has been shown to reduce SOA yields for some anthropogenic alkanes (Li et al., 2019b), aromatics (Ng et al., 2007a; Chan et al., 2009; Zhou et al., 2019), monoterpenes (Zhao et al., 2018) and other terpenes (Ng et al., 2007b), attributable to the formation of higher volatility products (e.g., organic nitrates) generated by RO_2 + NO compared to RO_2 + HO_2 (Presto et al., 2005; Li et al., 2019b), which is also likely the case here. The higher volatility products favor partitioning in the gas phase, thus reducing the potential for forming SOA (Zhou et al., 2019). Moreover, high NO_x levels can suppress the formation of products for nucleation, thereby reducing aerosol surface as a condensational sink and increasing the wall loss of condensable species in an OFR under high-NO_x conditions (Zhao et al., 2018; Sarrafzadeh et al., 2016; Wildt et al., 2014). Figure S5 indicates that the difference between SOA yields with and without NO_x decreased with increasing silicon atoms within individual cVMS, indicating a less restricting effect of NO_x on the SOA formation for larger cVMS. This means that high NO_x levels play a lessor role in the SOA yields of lower volatility precursors.

SOA yields in the AS-seeded experiments under low and high-NO_x conditions are also shown in Figs. 1 and S5, indicating minimal impacts of the AS seed particles on SOA yields. A yield enhancement ratio

($R_E = Y_{seeded}/Y_{unseeded}$, Fig. S6) was used to show the seed impacts more clearly. Under low-NO_x conditions, the R_E values for all cVMS were close to 1.0 (Fig. S6a), suggesting negligible impact of AS seed particles on SOA yields; however, under high-NO_x conditions, R_E was much larger (17.81, 13.18 and 15.51 for D3-D5, respectively) at short PA but gradually decreased to 1.0 with increasing PA for D3-D5, while it was always close to 1.0 for D6 regardless of PA (Fig. S6b). R_E values greater than 1.0 suggest that AS seed particles played an enhancement role in the cVMS SOA formation, as similarly reported in SOA formation from hydrocarbons (Sarrafzadeh et al., 2016; Lamkaddam et al., 2017; Li et al., 2019b). Under low-NO_x conditions, the general lack of impact on cVMS SOA yields by the AS seed particles suggests that condensation was not the main process driving SOA formation in cVMS oxidation. For the few cases of high NO_x level at low PA, where R_E was >1 for D3-D5, it is possible that their early generations of oxidation products were more volatile than successive generations of products and hence more prone to condensation enhanced by AS seeds. As PA increased, further reactions of these early generation oxidation products with OH radicals resulted in further generation products that were likely less volatile, thereby weakening the enhancing role of AS seeds at high OH exposure. Such effect was less pronounced for D6, likely because its oxidation products at different PA had similar volatilities. Figure S6b shows that the effect of AS seed particles on SOA yields negatively correlated with the number of silicon atoms in the cVMS. Lower volatility precursors (D5 and D6) may form lower volatile products, resulting in SOA yields less sensitive to the pre-existing seeds. In fact, most D5 oxidation products have been shown to be nearly non-volatile (Janechek et al., 2019; Wu and Johnston, 2017; Alton and Browne, 2020; Alton and Browne, 2022).

3.2 Aerosol compositions

3.2.1 Compositions of SOA under low-NO_x conditions.

Figures 2 and S7 show the normalized HR-ToF-AMS mass spectra of cVMS SOA from unseeded

experiments under low-NO_x conditions at OH exposures of 9.0×10^{11} molecules cm^{-3} s (i.e., OH concentration of 7.5×10^9 molecules cm^{-3}). The mass spectral signals can be identified as fragments with a formula of $C_xH_yO_zSi_n$. For D3 SOA, the most prominent peaks were at m/z 44 and 29, dominated by CO_2^+ and CHO^+, which were tracers for organic acids (Ng et al., 2010), alcohols and aldehydes (Lee et al., 2012), respectively. They may result from the oxidation of the methyl groups in D3 by OH radicals. For the mass spectra of D4-D6 SOA, the two highest peaks at m/z 14 and 15 were CH_2^+ and CH_3^+, respectively. In addition, there were several dominant $C_xH_yO_zSi_n$ peaks, which were fragments of silicon-containing products. For the $C_xH_yO_zSi_n$ group in D4 SOA, there were four typical peaks at m/z 255, 257, 271 and 273, with formulae of $C_4H_{11}O_7Si_3^+$, $C_3H_9O_8Si_3^+$, $C_3H_7O_9Si_3^+$ and $C_3H_9O_9Si_3^+$, respectively. The $C_xH_yO_zSi_n$ fragment group containing Si of D5 SOA had three dominant peaks at m/z 327, 329 and 331, corresponding to $C_{12}H_{11}O_2Si_5^+$, $C_9H_9O_8Si_3^+$ and $C_5H_{15}O_9Si_4^+$, respectively. For the $C_xH_yO_zSi_n$ group containing Si in D6 SOA, there were five main peaks at m/z 73 (C_3H_9Si), 387 ($C_8H_{23}O_8Si_5^+$), 389 ($C_8H_9O_9Si_5^+$), 401 ($C_9H_{21}O_{10}Si_4^+$) and 403 ($C_7H_{15}O_{12}Si_4^+$).

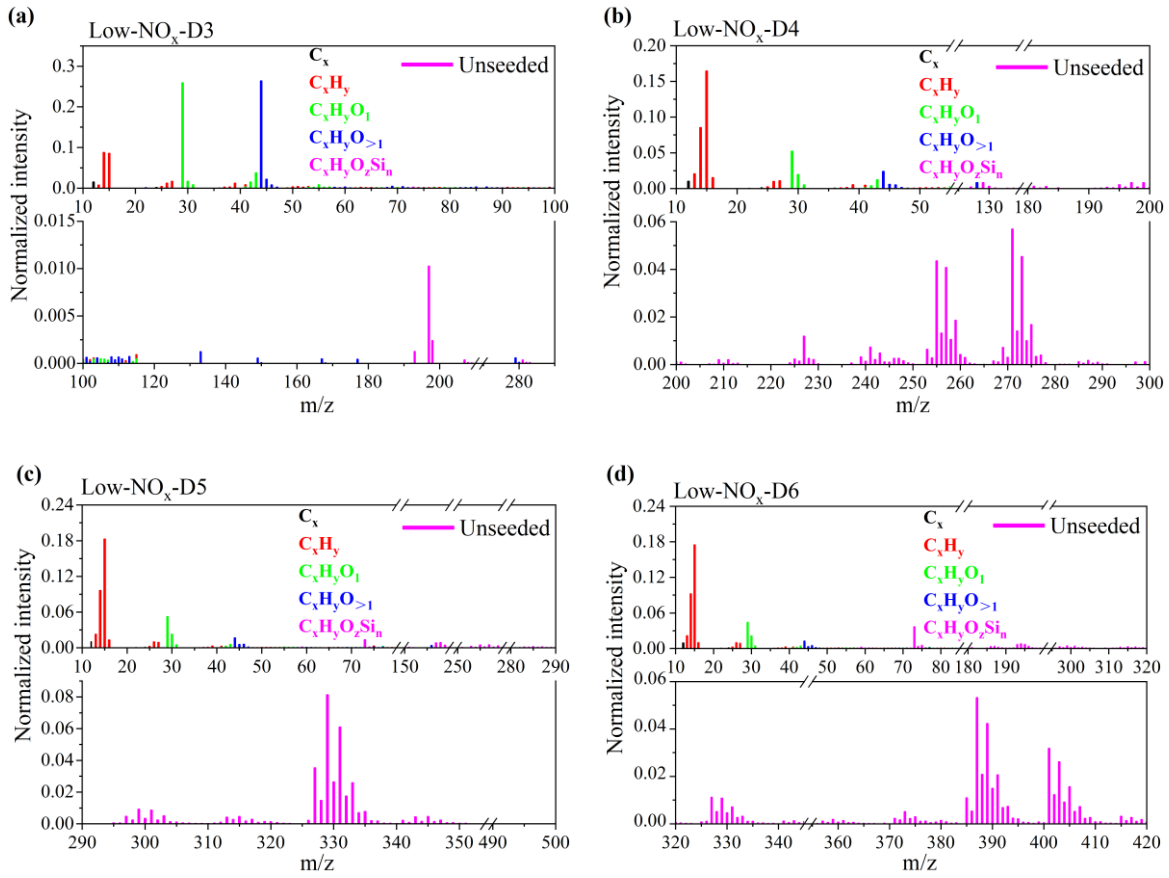

Figure 2. HR-ToF-AMS mass spectra of cVMS SOA at OH exposure of 9.0×10^{11} molecules cm^{-3} s (i.e., OH concentration of 7.5×10^{9} molecules cm^{-3}) under low-NO_x conditions in unseeded experiments. **a-d** represent the mass spectra of D3-D6 SOA, respectively.

Figure 3 shows the evolution of different groups of ions in the HR-ToF-AMS spectra of the cVMS SOA as a function of PA in equivalent days. For D3-D6 under unseeded conditions, $C_xH_yO_1$ and $C_xH_yO_{>1}$ ions significantly decreased within 0-4 equivalent days of PA, but remained essentially unchanged when PA increased to 7-15 equivalent days. The C_xH_y ion increased to its peak value at about 9 equivalent days of PA for D3 and 2-3 equivalent days of PA for D4-D6, and then gradually decreased with further PA increases. The $C_xH_yO_zSi_n$ group of ions maintained an increasing trend until 9-10 days of PA, thereafter it decreased slightly for D4-D6 SOA.

The weighted values of the atomic number ratios Si/C (n/x) and Si/O (n/z) for the $C_xH_yO_zSi_n$ groups in D5 and D6 SOA at different PA are plotted in Fig. S8 (Detailed calculations in Text S1 of the Supplement), which can be used to indicate the changes in the Si element of SOA. The Si/C ratio at initial SOA formation stage was close to that (0.50) in D5 and D6 molecules, and then increased continuously with increasing PA. The Si/O ratio kept increasing from 0.53 to 1.15 for D5 SOA and from 0.72 to 1.32 for D6 SOA, but varying around 1.0 that was the Si/O ratio in D5 and D6. While it is difficult to separate the effect of fragmentation due to the AMS ionization process, the relative changes of group intensities and the evolution of Si/C and Si/O in $C_xH_yO_zSi_n$ over different PA may be attributed to the evolution of cVMS when oxidized by the OH radicals. The initial step of OH radical oxidation is H abstraction from the methyl groups on the -Si-O- ring of the cVMS to form Si-containing radicals, which may generate OH and CH_2OH substitution products, such as silanol and silyl methanol (Wu and Johnston, 2016; Alton and Browne, 2020). Such Si-containing products may partition into SOA and result in an appearance of $C_xH_yO_zSi_n$ ions in the AMS mass spectra. Notably, it was reported that one of oxidation products of D5, 1- hydroxynonamethylcyclopentasiloxane (D_4TOH), has been detected in ambient particulate matter (Milani et al., 2021). At low PA, some oxygen-containing functional groups (-CH_2OH/-COOH/-OH), which were formed by the reaction of methyl groups in cVMS with OH, resulted in a small Si/O ratio (D5: 0.53; D6: 0.72) compared to that (1.0) in cVMS. With increasing PA, these functional groups (-CH_2OH/-COOH/-OH) may dissociate, leading to an increase in the Si/O ratio. The Si-O bond breaking may mainly happen at high OH exposures, and it may occur after the cleavage of S-C bonds (Rücker and Kümmerer, 2015). According to the previous study of Wu and Johnston(2017), some ring-opened products were generated from the reaction of D5 with OH radicals, necessarily requiring the cleavage of Si-O bonds. The Si-O bond cleavage from the OH radical attack may reduce the number of O atoms, leading to an increase of Si/O at high PA. The continued breaking of Si-O bonds would lead to

fragmentation and more volatile products, which caused lower SOA yield and $C_xH_yO_zSi_n$ fraction at longer PA (Figs. 1 and 3).

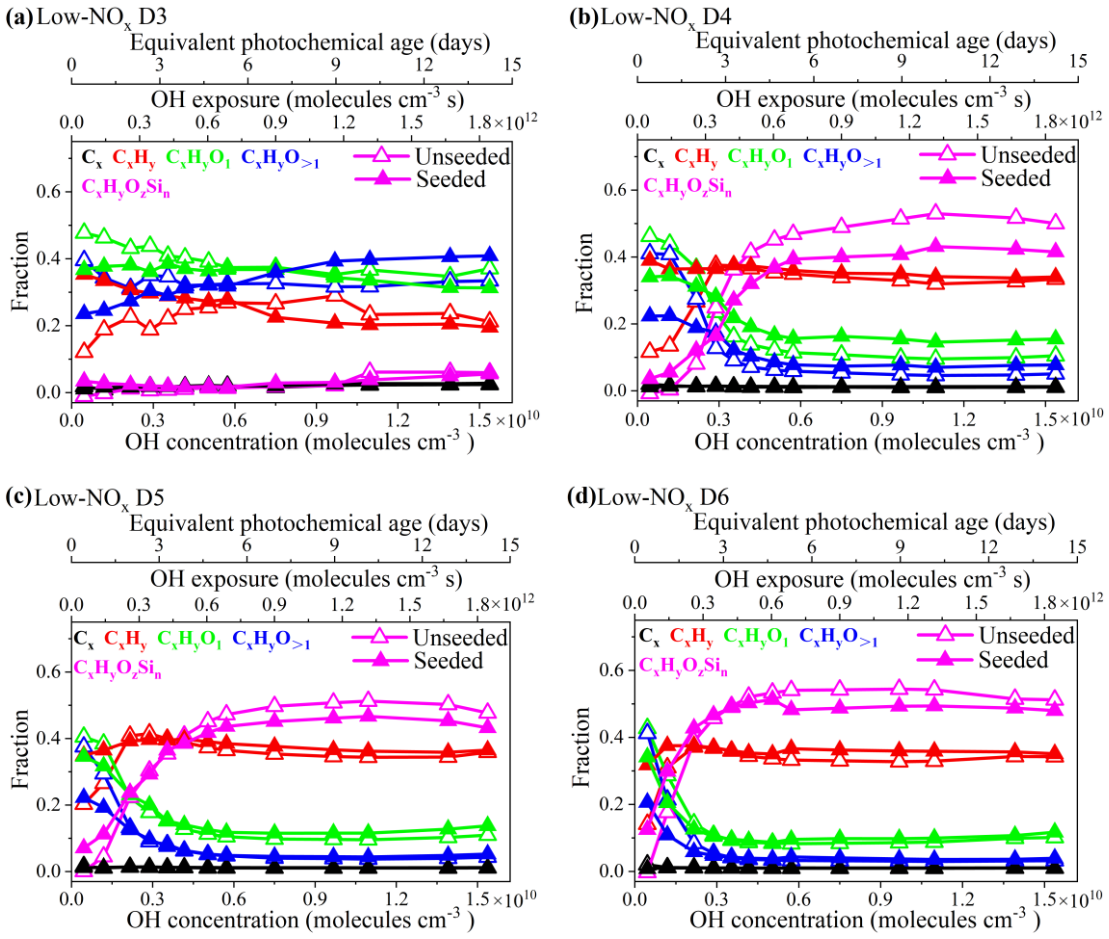

Figure 3. Fraction of C_x, C_xH_y, $C_xH_yO_1$, $C_xH_yO_{>1}$ and $C_xH_yO_zSi_n$ ion groups for SOA derived from the oxidation of cVMS (**a-d**) by OH radicals at different photochemical ages under low-NO_x conditions. Empty and solid triangles represent experimental data under unseeded and seeded conditions, respectively.

As shown in Fig. 3, the presence of seeds led to some changes in the evolution trends of ion groups in the AMS spectra. For instance, the initial fraction of C_xH_y in seeded experiments was larger than that in unseeded experiments, which may be related to the volatility of species containing C_xH_y that may be more easily deposited in the presence of seeds, whereas $C_xH_yO_1$ and $C_xH_yO_{>1}$ exhibited opposite changes. The presence of seeds led to larger initial and smaller steady-state $C_xH_yO_zSi_n$ fractions than those in unseeded experiments.

Regardless of the presence of seeds, C_xH_y, $C_xH_yO_1$ and $C_xH_yO_{>1}$ mainly contributed to the composition of all cVMS SOA at initial OH radicals oxidation, but D4-D6 SOA primarily consisted of C_xH_y and $C_xH_yO_zSi_n$ after 6 equivalent days.

3.2.2 Compositions of SOA under high-NO_x conditions.

Figure S9 shows the HR-ToF-AMS mass spectra of cVMS SOA from unseeded experiments under high-NO_x conditions at OH exposures of 9.0×10^{11} molecules cm^{-3} s (~6.9 d). Compared to that under low-NO_x conditions (Figs. 2 and S7), there was one additional N-containing group (N_mO_z) in the SOA mass spectra under high-NO_x conditions, which accounted for 16%-31%. For the mass spectra of D3-D6 SOA originating from unseeded experiments under high-NO_x conditions in Fig. S9, the dominating peaks of the N_mO_z family were m/z 30 (NO^+) and m/z 46 (NO_2^+). The common main peaks were located at m/z 30 (NO^+) for cVMS SOA, m/z 44 (CO_2^+) for D3-D4 SOA, and m/z 46 (NO_2^+) for D4-D6 SOA. In addition, there were other primary peaks at m/z 29 (CHO^+) for D4 SOA, while m/z 15 (CH_3^+) and m/z 28 (CO^+) for D5-D6 SOA. The m/z 28 (CO^+), similar with m/z 44 (CO_2^+), is considered as a tracer for organic acids (Ng et al., 2010). In the mass spectra for D3-D6 SOA under high-NO_x conditions, the presence of NO^+ (m/z 30) and NO_2^+ (m/z 46) illustrated the formation of organic or inorganic nitrates in SOA (Ng et al., 2007b; Zhao et al., 2018).

For the $C_xH_yO_zSi_n$ group in the D4 SOA mass spectrum under high-NO_x conditions, the dominating peaks and their formulas were same as those under low-NO_x conditions. For the $C_xH_yO_zSi_n$ group in D5 SOA, in addition to two typical peaks at m/z 327 and 329 in the low-NO_x experiments, there was another prominent peak at m/z 328, with a formula $C_8H_{12}O_5Si_5$. The $C_xH_yO_zSi_n$ group in D6 SOA had three typical peaks at m/z 73 (C_3H_9Si), m/z 387 ($C_8H_{23}O_8Si_5^+$) and m/z 401 ($C_9H_{21}O_{10}Si_4^+$). For the $C_xH_yO_zSi_n$ groups in cVMS SOA, there was little difference in the x, y, z and n value assignment of $C_xH_yO_zSi_n$ peaks in SOA generated under low-NO_x and high-NO_x conditions, suggesting the formation of similar Si-containing oxidation products.

For cVMS SOA under high-NO_x conditions, the evolution of family groups as a function of OH exposure was summarized in Fig. S10. The dominated composition at initial stage was $C_xH_yO_{>1}$ groups for D3-D6 SOA. At equivalent days larger than 6, D3 SOA primarily consisted of $C_xH_yO_{>1}$, N_mO_z and $C_xH_yO_1$ groups, while D4-D6 SOA was mainly composed of $C_xH_yO_zSi_n$, N_mO_z, $C_xH_yO_1$, C_xH_y and $C_xH_yO_{>1}$ groups. Figure S10 also shows influences of seeds on the evolution of family groups under high-NO_x conditions. It was observed that all groups in D3-D6 SOA displayed similar change trends regardless of the existence of seeds. As shown in Fig. S11, the trend of the weighted values of the atomic ratio Si/O in the $C_xH_yO_zSi_n$ groups at different photochemical ages under high-NO_x conditions was similar to that in low-NO_x experiments. However, the Si/C ratios remained almost unchanged, and were close to the initial value (0.5) in cVMS. This may be attributed to possible suppression of cleavage of methyl groups from the -Si-O- ring of the cVMS under high-NO_x conditions.

4 Conclusions and implications

The yields and compositions of SOA generated from the photooxidation of four cVMS (D3-D6) with OH radicals were investigated using an oxidation flow reactor. cVMS SOA yields exhibited an overall increasing trend with PA, and their values gradually increased with cVMS from D3 to D6. SOA formations depended on NO_x, as shown by smaller SOA yields under high-NO_x conditions. Ammonium sulfate seeds significantly enhanced SOA yields of D3-D5 at short PA under high-NO_x conditions. The SOA mass spectra showed that Si-containing species were one of main chemical compositions at PA of >6 days.

To evaluate the potential contributions of cVMS to SOA formation in the atmosphere, global SOA concentrations produced from cVMS were estimated according to the cVMS SOA yields measured in this work and using the cVMS concentrations reported from multiple studies, which were listed in Table S6. Here, the high-NO_x SOA yields under the seeded conditions at 8.5 equivalent days (D3: 0.028; D4: 0.122;

D5: 0.441; D6: 0.792) are employed in the calculation of cVMS SOA concentrations at urban sites, while the low-NO_x SOA yields under the unseeded conditions at 14.2 equivalent days (D3: 0.148; D4: 0.556; D5: 0.805; D6: 0.975) are used to estimate cVMS SOA at background and polar sites. The SOA formation from the reaction of cVMS with OH would always occur when the airmass is transported from urban aeras to low-NO_x sites such as rural, forested, and polar regions. To simplify the estimation process, the SOA yields at the maximum equivalent days (8.5 days) here were used for the calculation of SOA generated by cVMS from urban areas, although 8.5 days are longer for the residence time of an airmass in an urban area.

It should be noted that OH concentrations and exposures have different effects on the reaction systems, leading to different SOA yields. OH concentration determines the cVMS+OH reaction rate and therefore the instantaneous cVMS SOA yield. In contrast, OH exposure of cVMS determines the time-integrated, or cumulative, cVMS SOA yield. For any OH concentration, if a cVMS is exposed to the OH for a short period of time, the cumulative SOA yield over the short exposure time will be small. From this perspective, exposure is a more relevant factor to atmospheric conditions because SOA yield under such conditions should be an integration of instantaneous yields over the lifetime of a precursor compound in the atmosphere. Hence, one can argue that exposure experiments such as ours, simulating exposure in the real atmosphere, that were conducted using OFR, should be more suitable for application to the ambient atmosphere. Nevertheless, the interchanges between OH concentrations and exposures have to be considered due to experimental limitations, especially an inability to carry out long-time (multiple days) experiments. When extrapolating the laboratory data to the real atmosphere, it is necessary to consider atmospherically relevant OH concentrations and exposures. Charan et al. (2022) have claimed that D5 SOA yields are strongly dependent on both OH concentrations and exposures, implying the simultaneous effects of OH concentrations and reaction time on SOA yields. OH exposures in this work were 0.05-1.85×10^{12} molecules

388 cm^{-3} s, which was within atmospheric OH exposure range of cVMS when considering half-lives (6-30 days)
389 of cVMS and average OH concentration (1.5×10^6 molecules cm^{-3}) in the atmosphere. Although there may
390 be some uncertainties in extrapolating our results to the real atmosphere, such as larger cVMS concentrations
391 and SOA yields, these extrapolations may still provide an estimation for understanding the SOA potential of
392 cVMS.

393 Figure 4 shows the global concentration distribution of SOA from four cVMS (D3-D6) at 36 sites
394 worldwide estimated by the Equation 4,

395 $$C_{\text{cVMS-SOA}} = C_{\text{cVMS}} \times \frac{\Delta C_{\text{cVMS}}}{C_{\text{in-cVMS}}} \times Y \quad (4)$$

396 where C_{cVMS} and $C_{\text{cVMS-SOA}}$ are the mass concentration of cVMS reported from literatures and cVMS SOA
397 estimated in global sites, respectively; $C_{\text{in-cVMS}}$ and ΔC_{cVMS} are the mass concentration of initial and lost
398 cVMS at the selected equivalent days during the experiments of this work, respectively (Table S7); Y is the
399 cVMS SOA mass yields mentioned above. It was noted that the estimations from the Equation 4 were based
400 on assumptions that the lost cVMS ratio is not affected by the cVMS concentration and the background
401 $C_{\text{cVMS-SOA}}$ is zero. Table S6 summarizes the details regarding sites and concentrations of cVMS SOA. The
402 derived concentrations of cVMS SOA varies significantly among urban, background and polar sites. The
403 total cVMS SOA concentrations in urban areas are the highest, up to 1324 ng/m^3. They are 18.9-428 and
404 13.8-138.8 ng/m^3 for background and Arctic sites, respectively. cVMS SOA concentrations in urban regions
405 of Asia (sites 29-36) and Europe (sites 26-28) are generally larger than that of North America (sites 20-25).
406 In China, the total cVMS SOA concentrations in urban sites range from 15.5 to 1324 ng/m^3. The main
407 precursors of cVMS SOA are different among Chinese cities. For three cities along the southeast coast of
408 China (Guangzhou, Macau and Foshan), the dominant precursors of cVMS SOA are D3 and D4, which are
409 related to industrial emissions of these two siloxanes in this region (Wang et al., 2001). For Dalian in China,

mainly D5 and D6 contribute to cVMS SOA, which have the highest concentrations among all sites. This can be attributed to the industrial production of D5 and D6 and the use of personal care products in Dalian (Li et al., 2020). In the other Chinese urban areas with reported cVMS concentrations (Lhasa, Golmud, Kunming and Yantai), the total cVMS SOA concentrations are considerably smaller than those in the urban areas above, with D5 acting as the main precursor, which may be ascribed to the relatively low population densities in these cities (Wang et al., 2018).

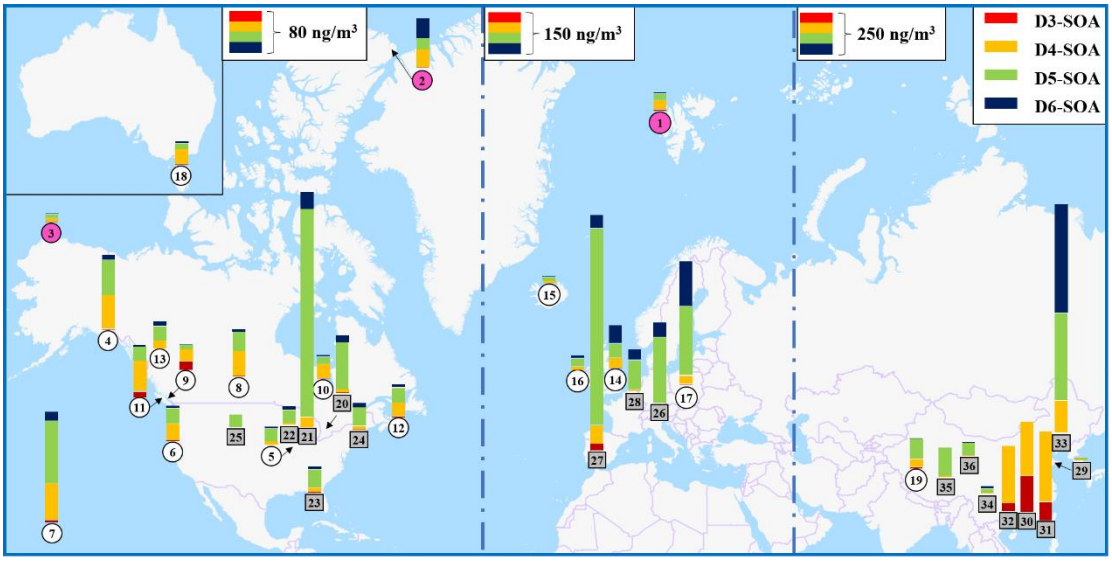

Figure 4. Global concentrations of cVMS SOA (ng/m^3) on the basis of the cVMS concentrations reported from multiple studies and the cVMS SOA yields measured in this work. The numbers of polar, background and urban sites are enclosed in pink, white circles and gray boxes, respectively. The details about cVMS and SOA concentrations at different sites were summarized in Table S6 of the Supplement.

At urban sites in Europe and North America, cVMS SOA concentrations are reported in the range of 138-813 ng/m^3 and 22.9-437 ng/m^3, respectively. Among these cVMS, D5 is the main contributor to cVMS SOA at these locations, averaging 80.1% of total cVMS SOA. This contribution is higher than that (73.6%) at Chinese urban sites. For instance, D5 SOA is calculated to be 684 ng/m^3 in Catalan, Spain, 387 ng/m^3 in

Chicago, USA, 229 ng/m^3 in Zurich, Switzerland and 99 ng/m^3 in Paris, France, where there are high levels of economic activities and high population densities. These results suggest that personal care products as a main source of D5 may be the most important anthropogenic origins of Si-containing SOA in Europe and North America. It was noted that the D5 SOA concentration (13.38-683.57 ng/m^3) estimated here is far more than that (0.016-0.206 ng/m^3) reported by Milani et al. (2021), who obtained their data using semi-quantified concentrations of D_4TOH (first-generation D5 SOA product) extracted from $PM_{2.5}$ samples in Atlanta and Houston. The difference may be mainly attributed to the missing analysis of multi-generation SOA products or dimers (Wu and Johnston, 2016, 2017). Pennington et al. (2021) utilized the developed CMAQ model to investigate the concentration of D5 SOA in the urban area of Los Angeles, and the model data (21 ng/m^3) was within these D5 SOA concentrations estimated here.

At background and Arctic sites, cVMS SOA are primarily derived from D4 and D5. The background sites are located in mountains, rural areas, forested areas, lakes and at high altitudes. The three highest cVMS SOA concentrations at background sites are located at Kosetice in the Czech Republic (428 ng/m^3), Hilo, Hawaii, USA (203 ng/m^3) and Tibetan Plateau in China (174 ng/m^3), where the contribution percentages of SOA from both D4 and D5 are 62.6%, 90.3% and 93.4%, respectively. The cVMS SOA concentrations at the Little Fox Lake site in Yukon, Canada is the highest (138.8 ng/m^3) among the four locations in the Arctic, 91% of which is accounted for by both D4 and D5 SOA. The dominance of D4 and D5 SOA in both background and the Arctic regions highlights their persistence in atmosphere and the potential for long-range atmospheric transport.

Furthermore, global concentration distribution of Si-containing SOA estimated for the four cVMS (D3-D6) at 36 sites worldwide is also presented in Table S6, which clearly shows the global importance of Si in SOA with the estimated percentages of cVMS SOA that contains the Si element. For example, up to 49.2%

448 and 31.2% of cVMS SOA contained Si elements in background and urban sites, respectively. These results
449 are similar to the summary observations that reported percentages of aerosols with a Si mole fraction >0.01
450 (%) at different sites (Bzdek et al., 2014). The above results demonstrated that Si is a frequent component of
451 SOA in background and urban areas.

452 The global annual production of D4, D5 and D6 is about 1, 0.1 and 0.01 $Tg \cdot yr^{-1}$, respectively, and 90% of
453 these cVMS is eventually released into the atmosphere (Li et al., 2020; Genualdi et al., 2011; Wang et al.,
454 2013; Sakurai et al., 2019). Based on the results shown in Fig. 4, the annual production of cVMS (D4-D6)
455 SOA was estimated to be 0.16 $Tg \cdot yr^{-1}$, which was about 5.5% of SOA (2.9 $Tg \cdot yr^{-1}$) produced from mobile
456 source emissions in the USA and 5-8 times of SOA generated by Athabasca oil sands (0.02-0.03 $Tg \cdot yr^{-1}$, one
457 of the largest sources of anthropogenic secondary organic aerosols in North America) (Tkacik et al., 2014;
458 Liggio et al., 2016). Moreover, it was also 0.8% and 2.3% of isoprene-SOA (20 $Tg \cdot yr^{-1}$) and monoterpenes-
459 SOA (7 $Tg \cdot yr^{-1}$) (typical biogenic SOA), respectively, indicating the potential importance of cVMS SOA
460 (Jokinen et al., 2015). While these cVMS SOA sources may seem small, they can make substantially higher
461 contributions to ambient air SOAs in population centers where cVMS compounds are primarily used.

462

463 **Author contributions**

464 CH designed and conducted all experiments; CH and HY analyzed the data and prepared the paper with
465 contributions from KL, PL, JL, AL and SML. SML supervised the project.

466

467 **Competing interests**

468 The authors declare that they have no conflict of interest.

469 **Acknowledgements**

This project was supported by Environment and Climate Change Canada's Climate and Clean Air Program (CCAP); the National Natural Science Foundation of China (42077198); the LiaoNing Revitalization Talents Program (XLYC1907185); the Fundamental Research Funds for the Central Universities (N2025011).

References

Ahrens, L., Harner, T., and Shoeib, M.: Temporal Variations of Cyclic and Linear Volatile Methylsiloxanes in the Atmosphere Using Passive Samplers and High-Volume Air Samplers, Environ. Sci. Technol., 48, 9374-9381, https://doi.org/10.1021/es502081j, 2014.

Allen, R., Kochs, P., and Chandra, G.: Industrial Organosilicon Materials, Their Environmental Entry and Predicted Fate, Springer, 3, 1-25, https://doi.org/10.1007/978-3-540-68331-5_1, 1997.

Alton, M. and Browne, E.: Atmospheric Chemistry of Volatile Methyl Siloxanes: Kinetics and Products of Oxidation by OH Radicals and Cl Atoms, Environ. Sci. Technol., 54, 5992-5999, https://dx.doi.org/10.1021/acs.est.0c01368, 2020.

Alton, M. W. and Browne, E. C.: Atmospheric Degradation of Cyclic Volatile Methyl Siloxanes: Radical Chemistry and Oxidation Products, ACS Environ. Au, XXX, XXX-XXX, https://doi.org/10.1021/acsenvironau.1c00043, 2022.

Atkinson, R.: Kinetics of the Gas-Phase Reactions of a Series of Organosilicon Compounds with OH and NO_3 Radicals and O_3 at 297 ± 2 K, Environ. Sci. Technol., 25, 863-866, https://doi.org/10.1021/es00017a005, 1991.

Bein, K., Zhao, Y., Wexler, A., Johnston, M.: Speciation of Size-Resolved Individual Ultrafine Particles in Pittsburgh, Pennsylvania, J. Geophys. Res., 110, D07S05, https://doi.org/10.1029/2004jd004708, 2005.

Berndt, T., Richters, S., Jokinen, T., Hyttinen, N., Kurtén, T., Otkjaer, R., Kjaergaard, H., Stratmann, F., Herrmann, H., Sipilä, M., Kulmala, M., and Ehn, M.: Hydroxyl Radical-Induced Formation of Highly Oxidized Organic Compounds, Nat. Commun., 7, 1-8, https://doi.org/10.1038/ncomms13677, 2016.

Bruns, E., Haddad, I., Keller, A., Klein, F., Kumar, N., Pieber, S., Corbin, J., Slowik, J., Brune, W., Baltensperger, U., and Prévôt, A.: Inter-Comparison of Laboratory Smog Chamber and Flow Reactor Systems on Organic Aerosol Yield and Composition, Atmos. Meas. Tech., 8, 2315-2332, https://doi.org/10.5194/amt-8-2315-2015, 2015.

Bzdek, B., Horan, A., Pennington, M., Janechek, N., Baek, J., Stanier, C., and Johnston, M.: Silicon is a Frequent

Component of Atmospheric Nanoparticles, Environ. Sci. Technol., 48, 11137-11145, https://doi.org/10.1021/es5026933, 2014.

Canada, E. C. a. H.: https://www.ec.gc.ca/ese-ees/FC0D11E7-DB34-41AA-B1B3-E66EFD8813F1/batch2_540-97-6_en.pdf last access: 9 February 2022, 2008.

Chan, A., Kautzman, K., Chhabra, P., Surratt, J., Chan, M., Crounse, J., Kürten, A., Wennberg, P., Flagan, R., and Seinfeld, J.: Secondary Organic Aerosol Formation from Photooxidation of Naphthalene and Alkylnaphthalenes: Implications for Oxidation of Intermediate Volatility Organic Compounds (IVOCs), Atmos. Chem. Phys., 9, 3049-3060, https://doi.org/10.5194/acp-9-3049-2009, 2009.

Chandramouli, B., Kamens, R.: The Photochemical Formation and Gas-Particle Partitioning of Oxidation Products of Decamethyl Cyclopentasiloxane and Decamethyl Tetrasiloxane in the Atmosphere, Atmos. Environ., 35, 87-95, https://doi.org/10.1016/S1352-2310(00)00289-2, 2001.

Charan, S., Huang, Y., Buenconsejo, R., Li, Q., Cocker Iii, D., and Seinfeld, J.: Secondary Organic Aerosol Formation from the Oxidation of Decamethylcyclopentasiloxane at Atmospherically Relevant OH Concentrations, Atmos. Chem. Phys., 22, 917-928, https://doi.org/10.5194/acp-22-917-2022, 2022.

Coggon, M., McDonald, B., Vlasenko, A., Veres, P., Bernard, F., Koss, A., Yuan, B., Gilman, J., Peischl, J., Aikin, K., DuRant, J., Warneke, C., Li, S.-M., and Gouw, J.: Diurnal Variability and Emission Pattern of Decamethylcyclopentasiloxane (D5) from the Application of Personal Care Products in Two North American Cities, Environ. Sci. Technol., 52, 5610-5618, https://doi.org/10.1021/acs.est.8b00506, 2018.

EUR-Lex: https://eur-lex.europa.eu/legal-content/EN/TXT/?uri=uriserv:OJ.L_.2018.006.01.0045.01.ENG&toc=OJ:L:2018:006:TOCECHA, last access: 25 November 2021, 2018.

Farasani, A. and Darbre, P.: Exposure to Cyclic Volatile Methylsiloxanes (cVMS) Causes Anchorage-Independent Growth and Reduction of BRCA1 in Non-Transformed Human Breast Epithelial Cells, J. Appl. Toxicol., 37, 454-461, https://doi.org/10.1002/jat.3378, 2017.

Genualdi, S., Harner, T., Cheng, Y., Macleod, M., Hansen, K., Egmond, R., Shoeib, M., and Lee, S.: Global Distribution of Linear and Cyclic Volatile Methyl Siloxanes in Air, Environ. Sci. Technol., 45, 3349-3354, https://doi.org/10.1021/es200301j, 2011.

Glasius, M. and Goldstein, A.: Recent Discoveries and Future Challenges in Atmospheric Organic Chemistry, Environ. Sci. Technol., 50, 2754-2764, https://doi.org/10.1021/acs.est.5b05105, 2016.

Guo, J., Zhou, Y., Cui, J., Zhang, B., and Zhang, J.: Assessment of Volatile Methylsiloxanes in Environmental

Matrices and Human Plasma, Sci. Total. Environ., 668, 1175-1182, https://doi.org/10.1016/j.scitotenv.2019.03.092, 2019.

Huang, Y., Coggon, M., Zhao, R., Lignell, H., Bauer, M., Flagan, R., and Seinfeld, J.: The Caltech Photooxidation Flow Tube reactor: Design, Fluid Dynamics and Characterization, Atmos. Meas. Tech., 10, 839-867, https://doi.org/10.5194/amt-10-839-2017, 2017.

Janechek, N., Hansen, K., and Stanier, C.: Comprehensive Atmospheric Modeling of Reactive Cyclic Siloxanes and their Oxidation Products, Atmos. Chem. Phys., 17, 8357-8370, https://doi.org/10.5194/acp-17-8357-2017, 2017.

Janechek, N., Marek, R., Bryngelson, N., Singh, A., Bullard, R., Brune, W., and Stanier, C.: Physical Properties of Secondary Photochemical Aerosol from OH Oxidation of a Cyclic Siloxane, Atmos. Chem. Phys., 19, 1649-1664, https://doi.org/10.5194/acp-19-1649-2019, 2019.

Jokinen, T., Berndt, T., Makkonen, R., Kerminen, V., Junninen, H., Paasonen, P., Stratmann, F., Herrmann, H., Guenther, A., Worsnop, D., Kulmala, M., Ehn, M., and Sipilä, M.: Production of Extremely Low Volatile Organic Compounds from Biogenic Emissions: Measured Yields and Atmospheric Implications, Proc. Natl. Acad. Sci. U S A., 112, 7123-7128, https://doi.org/10.1073/pnas.1423977112, 2015.

Kierkegaard, A. and McLachlan, M.: Determination of Linear and Cyclic Volatile Methylsiloxanes in Air at a Regional Background Site in Sweden, Atmos. Environ., 80, 322-329, https://doi.org/10.1016/j.atmosenv.2013.08.001, 2013.

Kim, J. and Xu, S.: Quantitative Structure-Reactivity Relationships of Hydroxyl Radical Rate Constants for Linear and Cyclic Volatile Methylsiloxanes, Environ. Toxicol. Chem., 36, 3240-3245, https://doi.org/10.1002/etc.3914, 2017.

Kim, J., Mackay, D., and Whelan, M.: Predicted Persistence and Response Times of Linear and Cyclic Volatile Methylsiloxanes in Global and Local Environments, Chemosphere, 195, 325-335, https://doi.org/10.1016/j.chemosphere.2017.12.071, 2018.

Krogseth, I., Zhang, X., Lei, Y., Wania, F., and Breivik, K.: Calibration and Application of a Passive Air Sampler (XAD-PAS) for Volatile Methyl Siloxanes, Environ. Sci. Technol., 47, 4463-4470, https://doi.org/10.1021/es400427h, 2013a.

Krogseth, I., Kierkegaard, A., McLachlan, M., Breivik, K., Hansen, K., and Schlabach, M.: Occurrence and Seasonality of Cyclic Volatile Methyl Siloxanes in Arctic Air, Environ. Sci. Technol., 47, 502-509, https://doi.org/10.1021/es3040208, 2013b.

Lambe, A., Chhabra, P., Onasch, T., Brune, W., Hunter, J., Kroll, J., Cummings, M., Brogan, J., Parmar, Y., Worsnop, D., Kolb, C., and Davidovits, P.: Effect of Oxidant Concentration, Exposure Time, and Seed Particles on Secondary Organic Aerosol Chemical Composition and Yield, Atmos. Chem. Phys., 15, 3063-3075, https://doi.org/10.5194/acp-15-3063-2015, 2015.

Lambe, A., Ahern, A., Williams, L., Slowik, J., Wong, J., Abbatt, J., Brune, W., Ng, N., Wright, J., Croasdale, D., Worsnop, D., Davidovits, P., and Onasch, T.: Characterization of Aerosol Photooxidation Flow Reactors: Heterogeneous Oxidation, Secondary Organic Aerosol Formation and Cloud Condensation Nuclei Activity Measurements, Atmos. Meas. Tech., 4, 445-461, https://doi.org/10.5194/amt-4-445-2011, 2011.

Lambe, A., Massoli, P., Zhang, X., Canagaratna, M., Nowak, J., Daube, C., Yan, C., Nie, W., Onasch, T., Jayne, J., Kolb, C., Davidovits, P., Worsnop, D., and Brune, W.: Controlled Nitric Oxide Production via $O(^1D) + N_2O$ Reactions for Use in Oxidation Flow Reactor Studies, Atmos. Meas. Tech., 10, 2283-2298, https://doi.org/10.5194/amt-10-2283-2017, 2017.

Lamkaddam, H., Gratien, A., Pangui, E., Cazaunau, M., Varrault, B., and Doussin, J.: High-NO_x Photooxidation of n-Dodecane: Temperature Dependence of SOA Formation, Environ Sci Technol, 51, 192-201, https://doi.org/10.1021/acs.est.6b03821, 2017.

Lee, A., Hayden, K., Herckes, P., Leaitch, W., Liggio, J., Macdonald, A., and Abbatt, J.: Characterization of Aerosol and Cloud Water at a Mountain Site During WACS 2010: Secondary Organic Aerosol Formation through Oxidative Cloud Processing, Atmos. Chem. Phys., 12, 7103-7116, https://doi.org/10.5194/acp-12-7103-2012, 2012.

Li, K., Liggio, J., Lee, P., Han, C., Liu, Q., and Li, S.-M.: Secondary Organic Aerosol Formation from α-Pinene, Alkanes, and Oil Sand-Related Precursors in a New Oxidation Flow Reactor, Atmos. Chem. Phys., 19, 9715-9731, https://doi.org/10.5194/acp-19-9715-2019, 2019a.

Li, K., Liggio, J., Han, C., Liu, Q., Moussa, S., Lee, P., and Li, S.-M.: Understanding the Impact of High-NO_x Conditions on the Formation of Secondary Organic Aerosol in the Photooxidation of Oil Sand-Related Precursors, Environ. Sci. Technol., 53, 14420-14429, https://doi.org/10.1021/acs.est.9b05404, 2019b.

Li, Q., Lan, Y., Liu, Z., Wang, X., Wang, X., Hu, J., and Geng, H.: Cyclic Volatile Methylsiloxanes (cVMSs) in the Air of the Wastewater Treatment Plants in Dalian, China-Levels, Emissions, and Trends, Chemosphere, 256, 1-8, https://doi.org/10.1016/j.chemosphere.2020.127064, 2020.

Li, S.-M. and Winchester, J.: Particle Size Distribution and Chemistry of Late Winter Arctic Aerosols, J. Geophys. Res., 95, 13897-13908, https://doi.org/10.1029/J095iD09p13897, 1990.

588 Li, S.-M. and Winchester, J.: Aerosol Silicon and Associated Elements in the Arctic High and Mid-Troposphere,
589 Atmos. Environ., 27, 2907-2912, https://doi.org/10.1016/0960-1686(93)90322-P, 1993.
590 Liggio, J., Li, S.-M., Hayden, K., Taha, Y., Stroud, C., Darlington, A., Drollette, B., Gordon, M., Lee, P., Liu, P.,
591 Leithead, A., Moussa, S., Wang, D., Brien, J., Mittermeier, R., Brook, J., Lu, G., Staebler, R., Han, Y., Tokarek,
592 T., Osthoff, H., Makar, P., Zhang, J., Plata, D., and Gentner, D.: Oil Sands Operations as a Large Source of
593 Secondary Organic Aerosols, Nature, 534, 91-94, https://doi.org/10.1038/nature17646, 2016.
594 Liu, N., Xu, L., and Cai, Y.: Methyl Siloxanes in Barbershops and Residence Indoor Dust and the Implication for
595 Human Exposures, Sci. Total. Environ., 618, 1324-1330, https://doi.org/10.1016/j.scitotenv.2017.09.250, 2018.
596 Mao, J., Ren, X., Brune, W., Olson, J., Crawford, J., Fried, A., Huey, L., Cohen, R., Heikes, B., Singh, H., Blake,
597 D., Sachse, G., Diskin, G., Hall, S., and Shetter, R.: Airborne Measurement of OH Reactivity during INTEX-
598 B, Atmos. Chem. Phys., 9, 163-173, https://doi.org/10.5194/acp-9-163-2009, 2009.
599 McFiggans, G., Mentel, T., Wildt, J., Pullinen, I., Kang, S., Kleist, E., Schmitt, S., Springer, M., Tillmann, R., Wu,
600 C., Zhao, D., Hallquist, M., Faxon, C., Breton, M., Hallquist, A., Simpson, D., Bergström, R., Jenkin, M., Ehn,
601 M., Thornton, J., Alfarra, M., Bannan, T., Percival, C., Priestley, M., Topping, D., and Scharr, A.: Secondary
602 Organic Aerosol Reduced by Mixture of Atmospheric Vapours, Nature, 565, 587-593,
603 https://doi.org/10.1038/s41586-018-0871-y, 2019.
604 Milani, A., Al-Naiema, I., and Stone, E.: Detection of a Secondary Organic Aerosol Tracer Derived from Personal
605 Care Products, Atmos. Environ., 246, https://doi.org/10.1016/j.atmosenv.2020.118078, 2021.
606 Ng, N., Kroll, J., Chan, A., Chhabra, P., Flagan, R., and Seinfeld, J.: Secondary Organic Aerosol Formation from
607 m-Xylene, Toluene, and Benzene, Atmos. Chem. Phys., 7, 3909-3922, https://doi.org/10.5194/acp-7-3909-2007,
608 2007a.
609 Ng, N., Chhabra, P., Chan, A., Surratt, J., Kroll, J., Kwan, A., McCabe, D., Wennberg, P., Sorooshian, A., Murphy,
610 S., Dalleska, N., Flagan, R., and Seinfeld, J.: Effect of NO_x Level on Secondary Organic Aerosol (SOA)
611 Formation from the Photooxidation of Terpenes, Atmos. Chem. Phys., 7, 5159-5174,
612 https://doi.org/10.5194/acp-7-5159-2007, 2007b.
613 Ng, N., Canagaratna, M., Zhang, Q., Jimenez, J., Tian, J., Ulbrich, I., Kroll, J., Docherty, K., Chhabra, P., Bahreini,
614 R., Murphy, S., Seinfeld, J., Hildebrandt, L., Donahue, N., DeCarlo, P., Lanz, V., Prévôt, A., Dinar, E., Rudich,
615 Y., and Worsnop, D.: Organic Aerosol Components Observed in Northern Hemispheric Datasets from Aerosol
616 Mass Spectrometry, Atmos. Chem. Phys., 10, 4625-4641, https://doi.org/10.5194/acp-10-4625-2010, 2010.
617 Peng, Z., Taylor, J., Orlando, J., Tyndall, G., and Jimenez, J.: Organic Peroxy Radical Chemistry in Oxidation

618 Flow Reactors and Environmental Chambers and their Atmospheric Relevance, Atmos. Chem. Phys., 19, 813-
619 834, https://doi.org/10.5194/acp-19-813-2019, 2019.
620 Peng, Z., Palm, B., Day, D., Talukdar, R., Hu, W., Lambe, A., Brune, W., and Jimenez, J.: Model Evaluation of
621 New Techniques for Maintaining High-NO Conditions in Oxidation Flow Reactors for the Study of OH-
622 Initiated Atmospheric Chemistry, ACS. Earth. Space. Chem. , 2, 72-86,
623 https://doi.org/10.1021/acsearthspacechem.7b00070, 2018.
624 Pennington, E., Seltzer, K., Murphy, B., Qin, M., Seinfeld, J., and Pye, H.: Modeling Secondary Organic Aerosol
625 Formation from Volatile Chemical Products, Atmos. Chem. Phys., 21, 18247-18261,
626 https://doi.org/10.5194/acp-21-18247-2021, 2021.
627 Phares, D., Rhoads, K., Johnston, M., and Wexler, A.: Size-Resolved Ultrafine Particle Composition Analysis 2.
628 Houston, J. Geophys. Res., 108, 1-14, https://doi.org/10.1029/2001jd001212, 2003.
629 Presto, A., Hartz, K., and Donahue, N.: Secondary Organic Aerosol Production from Terpene Ozonolysis. 2. Effect
630 of NO_x Concentration, Environ. Sci. Technol. , 39, 7046-7054, https://doi.org/10.1021/es050400s, 2005.
631 Rauert, C., Shoieb, M., Schuster, J., Eng, A., and Harner, T.: Atmospheric Concentrations and Trends of Poly- and
632 Perfluoroalkyl Substances (PFAS) and Volatile Methyl Siloxanes (VMS) over 7 Years of Sampling in the Global
633 Atmospheric Passive Sampling (GAPS) Network, Environ. Pollut., 238, 94-102,
634 https://doi.org/10.1016/j.envpol.2018.03.017, 2018.
635 Rhoads, K., Phares, D., Wexler, A., Johnston, M.: Size-Resolved Ultrafine Particle Composition Analysis 1.
636 Atlanta, J. Geophys. Res., 108, 1-13, https://doi.org/10.1029/2001jd001211, 2003.
637 Riipinen, I., Juuti, T., Pierce, J., Petäjä, T., Worsnop, D., Kulmala, M., and Donahue, N.: The Contribution of
638 Organics to Atmospheric Nanoparticle Growth, Nat. Geosci., 5, 453-458, https://doi.org/10.1038/ngeo1499,
639 2012.
640 Rücker, C. and Kümmerer, K.: Environmental Chemistry of Organosiloxanes, Chem. Rev., 115, 466-524,
641 https://doi.org/10.1021/cr500319v, 2015.
642 Safron, A., Strandell, M., Kierkegaard, A., and Macleod, M.: Rate Constants and Activation Energies for Gas-
643 Phase Reactions of Three Cyclic Volatile Methyl Siloxanes with the Hydroxyl Radical, Int. J. Chem. Kinet., 47,
644 420-428, https://doi.org/10.1002/kin.20919, 2015.
645 Sakurai, T., Imaizumi, Y., Kuroda, K., Hayashi, T., and Suzuki, N.: Georeferenced multimedia environmental fate
646 of volatile methylsiloxanes modeled in the populous Tokyo Bay catchment basin, Sci Total Environ, 689, 843-
647 853, https://doi.org/10.1016/j.scitotenv.2019.06.462, 2019.

Sarrafzadeh, M., Wildt, J., Pullinen, I., Springer, M., Kleist, E., Tillmann, R., Schmitt, S., Wu, C., Mentel, T., Zhao, D., Hastie, D., and Scharr, A.: Impact of NO_x and OH on Secondary Organic Aerosol Formation from β-Pinene Photooxidation, Atmos. Chem. Phys., 16, 11237-11248, https://doi.org/10.5194/acp-16-11237-2016, 2016.

Simonen, P., Saukko, E., Karjalainen, P., Timonen, H., Bloss, M., Saksa, P., Rönkkö, T., Keskinen, J., and Maso, M.: A New Oxidation Flow Reactor for Measuring Secondary Aerosol Formation of Rapidly Changing Emission Sources, Atmos. Meas. Tech., 10, 1519-1537, https://doi.org/10.5194/amt-10-1519-2017, 2017.

Sommerlade, R., Parlar, H., Wrobel, D , Kochs, P.: Product Analysis and Kinetics of the Gas-Phase Reactions of Selected Organosilicon Compounds with OH Radicals Using a Smog Chamber-Mass Spectrometer System, Environ. Sci. Technol., 27, 2435-2440, https://doi.org/10.1021/es00048a019, 1993.

Tang, X., Misztal, P., Nazaroff, W., and Goldstein, A.: Siloxanes Are the Most Abundant Volatile Organic Compound Emitted from Engineering Students in a Classroom, Environ. Sci. Technol. Lett. , 2, 303-307, https://doi.org/10.1021/acs.estlett.5b00256, 2015.

Tkacik, D., Lambe, A., Jathar, S., Li, X., Presto, A., Zhao, Y., Blake, D., Meinardi, S., Jayne, J., Croteau, P., and Robinson, A.: Secondary Organic Aerosol Formation from in-Use Motor Vehicle Emissions Using a Potential Aerosol Mass Reactor, Environ. Sci. Technol., 48, 11235-11242, https://doi.org/10.1021/es502239v, 2014.

Wang, D.-G., Norwood, W., Alaee, M., Byer, J., and Brimble, S.: Review of Recent Advances in Research on the Toxicity, Detection, Occurrence and Fate of Cyclic Volatile Methyl Siloxanes in the Environment, Chemosphere, 93, 711-725, https://doi.org/10.1016/j.chemosphere.2012.10.041, 2013.

Wang, X., Schuster, J., Jones, K., and Gong, P.: Occurrence and Spatial Distribution of Neutral Perfluoroalkyl Substances and Cyclic Volatile Methylsiloxanes in the Atmosphere of the Tibetan Plateau, Atmos. Chem. Phys., 18, 8745-8755, https://doi.org/10.5194/acp-18-8745-2018, 2018.

Wang, X., Lee, S., Sheng, G., Chan, L., Fu, J., Li, X., Min, Y., and Chan, C.: Cyclic organosilicon compounds in ambient air in Guangzhou, Macau and Nanhai, Pearl River Delta, Appl. Geochemistry, 16, 1447-1454, https://doi.org/10.1016/S0883-2927(01)00044-0, 2001.

Wildt, J., Mentel, T., Scharr, A., Hoffmann, T., Andres, S., Ehn, M., Kleist, E., Müsgen, P., Rohrer, F., Rudich, Y., Springer, M., Tillmann, R., and Wahner, A.: Suppression of New Particle Formation from Monoterpene Oxidation by NO_x, Atmos. Chem. Phys., 14, 2789-2804, https://doi.org/10.5194/acp-14-2789-2014, 2014.

Wu, Y. and Johnston, M.: Molecular Characterization of Secondary Aerosol from Oxidation of Cyclic Methylsiloxanes, J. Am. Soc. Mass Spectrom., 27, 402-409, https://doi.org/10.1007/s13361-015-1300-1, 2016.

Wu, Y. and Johnston, M.: Aerosol Formation from OH Oxidation of the Volatile Cyclic Methyl Siloxane (cVMS)

Decamethylcyclopentasiloxane, Environ. Sci. Technol., 51, 4445-4451, https://doi.org/10.1021/acs.est.7b00655, 2017.

Xiao, R., Zammit, I., Wei, Z., Hu, W.-P., MacLeod, M., and Spinney, R.: Kinetics and Mechanism of the Oxidation of Cyclic Methylsiloxanes by Hydroxyl Radical in the Gas Phase: An Experimental and Theoretical Study, Environ. Sci. Technol., 49, 13322-13330, https://doi.org/10.1021/acs.est.5b03744, 2015.

Xu, S., Warner, N., Nizzetto, P., Durham, J., and McNett, D.: Long-Range Transport Potential and Atmospheric Persistence of Cyclic Volatile Methylsiloxanes Based on Global Measurements, Chemosphere, 228, 460-468, https://doi.org/10.1016/j.chemosphere.2019.04.130, 2019.

Zhao, D., Schmitt, S., Wang, M., Acir, I., Tillmann, R., Tan, Z., Novelli, A., Fuchs, H., Pullinen, I., Wegener, R., Rohrer, F., Wildt, J., Scharr, A., Wahner, A., and Mentel, T.: Effects of NO_x and SO_2 on the Secondary Organic Aerosol Formation from Photooxidation of α-Pinene and Limonene, Atmos. Chem. Phys., 18, 1611-1628, https://doi.org/10.5194/acp-18-1611-2018, 2018.

Zhou, C., Jang, M., and Yu, Z.: Simulation of SOA Formation from the Photooxidation of Monoalkylbenzenes in the Presence of Aqueous Aerosols Containing Electrolytes under Various NO_x Levels, Atmos. Chem. Phys., 19, 5719-5735, https://doi.org/10.5194/acp-19-5719-2019, 2019.